# Inhomogeneous optical absorption around the *K* point in graphite and carbon nanotubes

A. Grüneis,[1,2] R. Saito,[1,2] Ge. G. Samsonidze,[6] T. Kimura,[1] M. A. Pimenta,[3] A. Jorio,[3,4]
A. G. Souza Filho,[4,7] G. Dresselhaus,[5] and M. S. Dresselhaus[4,6]

[1]*Department of Electronic-Engineering, University of Electro-Communications, Chofu, Tokyo, 182-8585, Japan*
[2]*CREST, JST, ■, Japan*
[3]*Departamento de Física, Universidade Federal de Minas Gerais, Belo Horizonte–MG, 30123-970 Brazil*
[4]*Department of Physics, Massachusetts Institute of Technology, Cambridge, Massachusetts 02139-4307*
[5]*Francis Bitter Magnet Laboratory, Massachusetts Institute of Technology, Cambridge, Massachusetts 02139-4307*
[6]*Department of Electrical Engineering and Computer Science, Massachusetts Institute of Technology, Cambridge,
Massachusetts 02139-4307*
[7]*Departamento de Física, Universidade Federal do Ceará, Fortaleza-CE, 60455-760 Brazil*

The optical absorption spectra of $\pi$ electrons is calculated for graphite and carbon nanotubes. Particular attention is paid to the processes contributing to the optical absorption as a function of the **k** vector and light polarization direction. The optical absorption amplitude around the *K* point in the Brillouin zone has a node in the two-dimensional Brillouin zone of graphite. The formula for the absorption scattering matrix around the *K* point is given analytically by expanding the matrix element into a Taylor series. The chirality dependence of the absorption matrix element of a single carbon nanotube is presented.

## I. INTRODUCTION

The optical absorption is a fundamental property of a solid and is well described by its electronic energy band structure. Various works have been published on the optical absorption in graphite and carbon nanotubes, focusing on nanotube bundles[1–4] or on the dipole selection rules for optical transitions.[5,6] The polarization dependence of the Raman intensity for a single nanotube has also been discussed[7–11] in which the optical absorption is suppressed for the polarization of light perpendicular to the nanotube axis. The absence of optical absorption for light polarization perpendicular to the nanotube axis comes from the following facts: (1) the dipole selection rules give different absorption energies for the polarization parallel and perpendicular to the nanotube axis, and (2) the depolarization effect screens the electric field through a self-consistent induced charge. Here we present a new result on the optical absorption of carbon nanotubes, obtained by calculating the absorption matrix element. This result is independent of previous work and is closely related to resonance Raman spectroscopy.[12,13]

Generally, optical transitions occur *vertically*, connecting an occupied energy band to an unoccupied one with almost the same wave vector as a result of energy-momentum conservation of light and of the electron. The optical spectra are generally presented as a function of energy, but are not so often given as a function of the **k** vector of the electron. This is simply because the optical absorption is given by all possible contributions of the electrons with different **k** vectors in the Brillouin zone (BZ). However, the **k** dependence of the optical absorption may be important in the case of nanographite ribbons and carbon nanotubes, in which some singular **k** vectors are related to the two-dimensional (2D) **k** vector in the 2D BZ when it is folded into the 1D BZ.[14]

Such an idea is motivated by recent resonance Raman experiments on isolated single-wall carbon nanotubes

(SWNT's).[7,15] As far as we know, all resonance Raman intensities have been calculated with the assumption that the absorption matrix element does not change much as a function of energy or **k**. In this paper we show that this assumption is not always correct, but rather there is a node in the amplitude of the absorption matrix element for graphite as a function of **k** for certain polarization directions of the light. This result might be important for explaining the *D*-band and *G*'-band spectra of $(n,m)$ nanotubes for which special electron **k** vectors are selected in the various double-resonance Raman processes.[16–19]

In order to discuss the resonance Raman intensity quantitatively, we need to consider both electron-photon nd electron-phonon matrix elements. However, in this paper we mainly focus our attention on the dipole transition probability of the electron in the BZ. With only these results, we can still obtain much important information about the discussion of the photoabsorption process in graphite and in carbon nanotubes.

In the next section, using the standard theory of electric dipole transitions in solids, we can formulate the absorption amplitude for graphite and carbon nanotubes using tight-binding wave functions and linearly polarized light. Using the eigenfunctions around the *K* and *K*' points in the 2D BZ, we obtain an analytic form for the optical absorption. In Sec. III, we give the calculated results for the optical absorption of graphite. In Sec. IV, we predict the chirality dependence of the optical absorption matrix element for an $(n,m)$ SWNT. In Sec. V, the conclusion of this paper is presented.

## II. OPTICAL ABSORPTION FORMULA FOR GRAPHITE

The optical absorption for a laser energy less than 3 eV corresponds to $\pi$-$\pi$* transitions in graphite and in carbon nanotubes. The dipole selection rule tells us that an optical transition for the $2p$ orbitals on the same lattice site is not

possible. However, the transition from a $2p$ orbital of one atom to that of the neighboring atom is possible, which gives the $\pi$-$\pi^*$ transitions in graphite and in carbon nanotubes. Because of the large overlap between $\pi$ orbitals, this interatomic transition is commonly observed experimentally. First-order time-dependent perturbation theory gives the following formula for the absorption probability per unit time $W(\mathbf{k})$ for an electron with wave vector $\mathbf{k}$:

$$W(\mathbf{k}) = \frac{4e^2\hbar^4 I}{\tau \epsilon m^2 c^3 E_{\text{laser}}^2} |\mathbf{P} \cdot \langle \Psi^c(\mathbf{k})|\nabla|\Psi^v(\mathbf{k})\rangle|^2$$

$$\times \frac{\sin^2[E_c(\mathbf{k})-E_v(\mathbf{k})-E_{\text{laser}}]\tau/2\hbar}{[E_c(\mathbf{k})-E_v(\mathbf{k})-E_{\text{laser}}]^2}, \qquad (1)$$

where the $\Psi^c$ and $\Psi^v$ ($E_c$ and $E_v$) are the wave functions (energies) of the valence and conduction bands, respectively, $\mathbf{P}$ is the polarization vector of light, and $E_{\text{laser}}$, $I$, $\epsilon$, $m$, and $\tau$ are, respectively, the incident laser energy and intensity, dielectric constant, mass of the electron, and the time used for taking the average. The value of $\tau = \Delta x/c = 2\pi/\Delta\omega$ is determined by the uncertainty relation and the width of the incident laser frequency $\Delta\omega$. Typical values of $\tau$ for $\Delta\omega = 10$ cm$^{-1}$ correspond to 0.5 ps. If we take a sufficiently large value for $\tau$, the function $\sin^2 X/X^2$ ($X = [E_c(\mathbf{k}) - E_v(\mathbf{k}) - E_{\text{laser}}]\tau/2\hbar$), appearing in the second line of Eq. (1), becomes the delta function $\delta(E_c(\mathbf{k}) - E_v(\mathbf{k}) - E_{\text{laser}})$, and Eq. (1) is known as Fermi's golden rule. The total absorption probability per unit time is obtained by integrating $W(\mathbf{k})$ on $\mathbf{k}$ over the 2D (or 1D) BZ. $\Psi_c$ and $\Psi_v$ can be written as a sum of the two Bloch functions consisting of the two carbon atoms $A$ and $B$ in the 2D graphite unit cell,[14] $\Phi_j(\mathbf{k},\mathbf{r})$ ($j=A,B$),

$$\Psi^i(\mathbf{k},\mathbf{r}) = \sum_{j=A,B} C_j^i(\mathbf{k})\Phi_j(\mathbf{k},\mathbf{r}), \quad (i=c,v), \qquad (2)$$

where $C_j^i(\mathbf{k})$ is the coefficient of the Bloch functions obtained by solving the two-dimensional Hamiltonian and overlap matrices for 2D graphite[14] for $H$ and $S$:

$$H\mathbf{C} = ES\mathbf{C}. \qquad (3)$$

In the tight-binding method, the Bloch functions for the $\pi$ band, $\Phi_j(\mathbf{kr})$ ($j=A,B$), are expressed by a linear combination of atomic $2p_z$ orbitals at $\mathbf{r}=\mathbf{R}_j$, $\phi(\mathbf{r}-\mathbf{R}_j)$, in the solid ($N$ atoms):

$$\Phi_j(\mathbf{k},\mathbf{r}) = \frac{1}{\sqrt{N}} \sum_{\mathbf{R_j}}^N e^{i\mathbf{k}\cdot\mathbf{R}_j}\phi(\mathbf{r}-\mathbf{R}_j) \quad (j=A,B). \qquad (4)$$

Putting Eqs. (2) and (4) into Eq. (1), the absorption amplitude is given by a linear combination of atomic matrix elements. Since the matrix element for the same atomic orbital, $\langle \phi(\mathbf{r}-\mathbf{R}_j)|\nabla|\phi(\mathbf{r}-\mathbf{R}_j)\rangle = \mathbf{0}$, becomes a zero vector, the leading term of Eq. (1) comes from the pairs of the nearest-neighbor $A$ and $B$ carbon atoms.

When we put a graphene layer on the $xy$ plane, then all the atomic matrix elements between two atoms $j1$ and $j2$ for the derivative on $z$ become zero,

$$\langle \phi(\mathbf{r}-\mathbf{R}_{j1})|\frac{\partial}{\partial z}|\phi(\mathbf{r}-\mathbf{R}_{j2})\rangle = 0, \qquad (5)$$

because the integrand is an odd function of $z$. Here we use the fact that the $2p_z$ orbital $\phi(\mathbf{r}-\mathbf{R}_j)$ is given by the product of $z$ and a radial function $R_{2p}(|\mathbf{r}-\mathbf{R}_j|)$, when $R_{2p}$ and its derivative can be expressed by a sum of some Gaussian functions at $\mathbf{r}=\mathbf{R}_j$ and the values do not have nodes around the nearest-neighbor atoms.

The matrix element for the derivative on $x$ (or $y$) has a nonvanishing value if the relative position $\mathbf{R}_{j1} - \mathbf{R}_{j2}$ has an $x$ (or $y$) component. When we consider the matrix elements only for the three nearest-neighbor atoms, we can get the formulation

$$\langle \Psi_c(\mathbf{k})|\nabla|\Psi_v(\mathbf{k})\rangle = \frac{2\sqrt{3}M}{a}\text{Re}\left[ C_A^{c*}(\mathbf{k})C_B^v(\mathbf{k})\sum_{i=1}^3 e^{i\mathbf{k}\cdot\mathbf{b}_i}\mathbf{b}_i \right], \qquad (6)$$

where $a=2.46$ Å is the lattice constant of 2D graphite, Re $[\cdots]$ is the real part of $[\cdots]$, and $\mathbf{b}_i$ ($i=1,3$) are the nearest-neighbor carbon atom vectors from $B$ to $A$ sites. $\mathbf{b}_1 = (-a_{\text{C-C}},0,0)$ with a bond length $a_{\text{C-C}}=a/\sqrt{3}=1.42$ Å, while $\mathbf{b}_2$ and $\mathbf{b}_3$ are given by rotating $\mathbf{b}_1$ by $2\pi/3$ and $4\pi/3$, respectively. It is noted that we used for Eq. (6) the relation $C_A^{v*}C_B^c = -(C_B^{v*}C_A^c)^*$, which can be directly shown by the analytic form of $C_j^i$. Also $M$ in Eq. (6) is the optical matrix element for the two nearest-neighbor atoms separated by $\mathbf{b}_1$:

$$M = \langle \phi(\mathbf{R}+\mathbf{b}_1)|\frac{\partial}{\partial x}|\phi(\mathbf{R})\rangle. \qquad (7)$$

For light with energy smaller than 3 eV, the optical absorption occurs around the $K$ and $K'$ points (hexagonal corners) of the 2D BZ. In this case, Eq. (6) is expanded as a Taylor series in $\mathbf{k}$ around the $K$ points. This expression is useful to understand the present new physics. Hereafter all coordinates of $\mathbf{k}$ in the Taylor expansions are measured from the $K$ point. The wave vector coefficients can be expressed as a linear function of $\mathbf{k}$.[20,21] Hereafter we assume that the overlap matrix $S$ of Eq. (3) is simply the unit matrix. In this case, the normalization condition of the wave functions is given by

$$C_A^{i*}(\mathbf{k})C_A^j(\mathbf{k}) + C_B^{i*}(\mathbf{k})C_B^j(\mathbf{k}) = \delta_{ij} \quad (i,j=c \text{ or } v), \qquad (8)$$

where $\delta_{ij}$ is either 1 or 0 for $i=j$ and $i\neq j$, respectively. The coefficients of the wave function are expanded around $K(K')$ as

$$C_A^c(\mathbf{k}) = \frac{1}{\sqrt{2}}, \quad C_B^c(\mathbf{k}) = \frac{\pm k_y - ik_x}{\sqrt{2}k},$$

$$C_A^v(\mathbf{k}) = -\frac{1}{\sqrt{2}}, \quad C_B^v(\mathbf{k}) = \frac{\pm k_y - ik_x}{\sqrt{2}k}, \qquad (9)$$
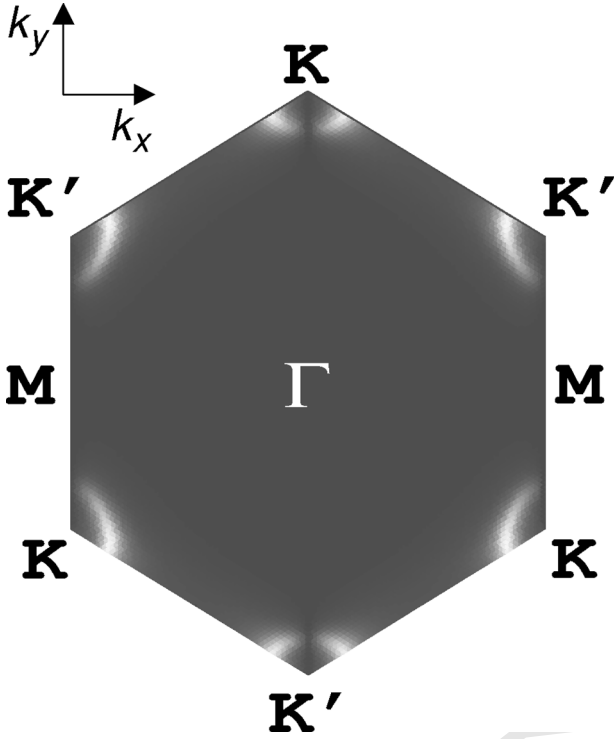
FIG. 1. Plot of the optical absorption intensity $W(\mathbf{k})$ over the two-dimensional BZ of graphite. The polarization vector and the laser energy are selected as $\mathbf{P}=(0,1)$ and $E_{\text{laser}}=3$ eV, respectively. For better visibility, the thickness of the lines around $K$ has been increased. It can be seen that the absorption is zero along the vertical lines connecting the $K$ and $K'$ points.

where $k=\sqrt{k_x^2+k_y^2}$ is the distance from the $K$ or $K'$ point. Here the plus (minus) sign for the $k_y$ value is valid for the expansion around the $K(K')$ point. The coordinates of the two inequivalent $K$ points in the BZ are $K=(0,4\pi/3a)$ and $K'=(0,-4\pi/3a)$, respectively (see Fig. 1). The expression for the $K'$ point can be easily obtained by the relation $C_j^i(\mathbf{k})=C_j^{i*}(-\mathbf{k})$. Similarly, by expanding $e^{i\mathbf{k}\cdot\mathbf{b}_i}\mathbf{b}_i$ appearing in Eq. (6) around the $K$ and $K'$ points, we get the following result for the numerator of Eq. (1) up to the linear terms in $k_x$ and $k_y$ for a given polarization vector $\mathbf{P}=(p_x,p_y)$:

$$\mathbf{P}\cdot\langle\Psi_c(\mathbf{k})|\vec{\nabla}|\Psi_v(\mathbf{k})\rangle=\pm\frac{3M}{2k}(p_y k_x - p_x k_y). \qquad (10)$$

This result shows that the line $p_y k_x - p_x k_y=0$ in the 2D BZ becomes a node in the optical absorption for a given $\mathbf{P}=(p_x,p_y)$. For a given laser energy, the equienergy line for optical absorption gives a circle around the $K$ point $k=E_{\text{laser}}/\sqrt{3}\gamma_0 a$ with $\gamma_0=2.89$ eV (Refs. 22 and 23) for optical experiments on carbon nanotubes. Thus we expect no optical absorption around the two crossing points of the line $p_y k_x - p_x k_y=0$ with the circle. This result holds for both the $K$ and the $K'$ points to first order; i.e., the location of the node rotates in the same direction by rotating the polarization

direction. However, higher-order terms modify this behavior, since the corrections for $K$ and $K'$ are different from each other.

The existence of a node in the absorption coefficient as a function of $\mathbf{k}$ is a special effect that has never been observed in other materials. It occurs in graphite because the linear terms of Eq. (10) depend only on the expressions of $C_j^i$ in Eq. (9), since for the case of 2D graphite (or carbon nanotubes) there are two equivalent carbon atoms in the unit cell and the energy dispersion is linear near the Fermi energy. In most materials, a quadratic term in $k_x$, $k_y$ is the leading term in the energy dispersion relation, so that the optical absorption then does not have a node. Nevertheless, it might be difficult to observe the existence of such a node in the optical absorption of graphite experimentally. We will next discuss the effect of the node for graphite and for carbon nanotubes in more detail in the following sections.

## III. CALCULATED RESULTS FOR GRAPHITE

In Fig. 1, we plot the absorption probability per unit time $W(\mathbf{k})$ of Eq. (1) in the 2D BZ of a graphene sheet for $E_{\text{laser}}=3$ eV and $\mathbf{P}=(0,1)$. The highlighted (bright) region gives a large absorption coefficient. It is clear from the figure that nodes in the optical absorption appear on the vertical lines connecting the $K$ and $K'$ points in the 2D BZ ($k_x=0$, $\pm 2\pi/\sqrt{3}a$). For a different polarization direction $\mathbf{P}=(1,0)$, the nodes appear on the horizontal lines connecting the $K$ and $K'$ points ($k_y=\pm 2\pi/3a$). Since we solve the wave functions numerically, the higher-order corrections for the node of Eq. (10) are included in Fig. 1.

As far as the linear $k$ approximation for the energy and the wave function is valid, the expression in Eq. (10) works well for specifying the node position. However, when the laser energy increases, the equienergy contour is no longer a circle, but is changed into a triangle by the trigonal warping effect.[24] In this case, the higher-order corrections for Eq. (10) become important for describing the node positions and the absolute value of $W(\mathbf{k})$. In Fig. 2, we plot $W(\mathbf{k})$ as a function of the polar angle $\phi$ of the node around the $K$ point, that is, $k_x=k\cos\phi$ and $k_y=k\sin\phi$, with $E_{\text{laser}}=2.5$ eV, for (a) $\mathbf{P}=(1,0)$ and (b) $\mathbf{P}=(0,1)$. Solid, dashed, and dotted lines in Fig. 2 correspond to numerical results obtained by solving the Hamiltonian in Eq. (3) and the analytic expression within the linear and quadratic $k$ approximations for Eq. (10), respectively. In the case of Fig. 2(a), $\phi=0,\pi$ (or $k_y=0$) correspond to the node positions of $W(\mathbf{k})$, while in the case of Fig. 2(b), $\phi=\pi/2,3\pi/2$ (or $k_x=0$) correspond to the node positions. In the case of (b), since $\phi=0$ and $\pi$ are equivalent $\mathbf{k}$ positions, the value of $W(\mathbf{k})$ is identical, while this is not the case for (a). It is clear from the figure that the linear approximation of Eq. (10) is sufficient for describing the node position for $E_{\text{laser}}<3$ eV; however, we need to use at least the quadratic term of $\mathbf{k}$ for describing the asymmetric
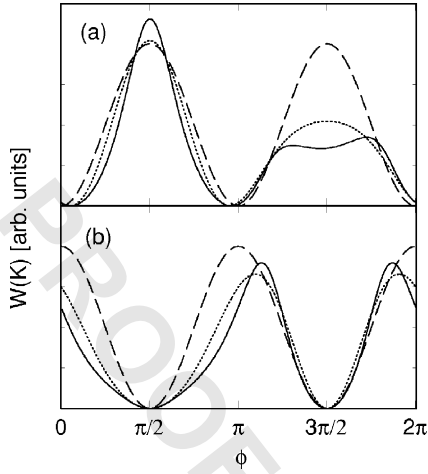
FIG. 2. The absorption probability $W(\mathbf{k})$ as a function of angle $\phi$ around the $K$ point. Solid, dashed, and dotted lines, respectively, denote the numerical results obtained from use of the eigenvectors and the linear and quadratic approximations in Eq. (10). The plots are made for $E_{\text{laser}}=2.5$ eV, and the polarization vectors are (a) $\mathbf{P}=(1,0)$ and (b) $\mathbf{P}=(0,1)$.

peaks of $W(\mathbf{k})$. This asymmetry will be important for describing the chirality dependence of $W(\mathbf{k})$ for SWNT's, as discussed in the next section.

## IV. OPTICAL ABSORPTION OF SINGLE-WALL CARBON NANOTUBES

The calculation of the SWNT optical absorption spectra can be based on Eq. (1). The dipole matrix element can be expressed by the sum of the dipole vector at each carbon atom. An important point to note is that the polarization vector $\mathbf{P}$ of the light for each carbon atom relative to the cylindrical surface of the nanotube is different from one another. In order to calculate the absorption by a given $A(B)$ atom of a SWNT, we need to rotate the atomic matrix element vector, $\langle \phi(\mathbf{r}-\mathbf{R}_j)|\nabla|\phi(\mathbf{r}-\mathbf{R}_j)\rangle$, around the axis perpendicular to the cylindrical surface ($U_y$; see below) and the nanotube axis ($U_z$), and before taking an inner product with the polarization vector $\mathbf{P}$. The $U_y$ rotation is needed for getting the chiral angle $\theta$ of a SWNT. Hereafter we denote the matrix element vector as the dipole vector, and we select the nanotube axis in the $z$ direction. When $\mathbf{P}$ is parallel to the $z$ axis, only the $z$ component of the dipole vector contributes to $W(\mathbf{k})$, while for $\mathbf{P}$ perpendicular to the $z$ axis, only the $x,y$ components of the dipole vector have a nonvanishing value when $\mathbf{k}-\mathbf{k}'=\pm\mathbf{K}_1$.[5] The corresponding dipole selection rule from $E_i^v \rightarrow E_j^c$ for the energy subbands of SWNT's is $i=j$ and $i=j\pm1$ for polarization parallel and perpendicular to the nanotube axis, respectively, where the subband indexes of $E_i^v$ and $E_j^c$ are taken symmetrically around the Fermi energy.

The explicit formulation of the absorption matrix element for a transition from $\mathbf{k}'$ to $\mathbf{k}$ is given by,
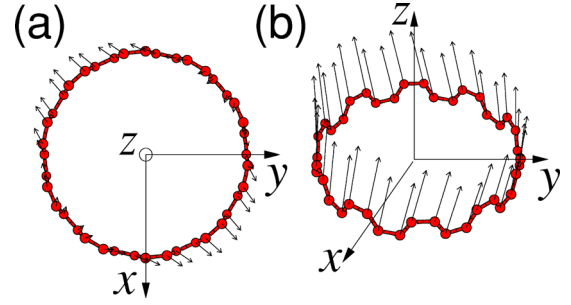


FIG. 3. (a) Top and (b) side views of the atomic dipole matrix vector (dipole vector) for a (10,10) carbon nanotube. The dipole vector for each atom has a large $z$ component which contributes to optical absorption for the polarization parallel to the nanotube axis ($z$), while the small $x$ and $y$ components contribute in the perpendicular polarization.

$$\langle \Psi^c(\mathbf{k})|\nabla|\Psi^v(\mathbf{k}')\rangle$$

$$=\frac{\sqrt{3}M}{Na}\Bigg[ C_A^{c*}(\mathbf{k})C_B^v(\mathbf{k}')\sum_j^N e^{i(\mathbf{k}-\mathbf{k}')\cdot R_j^B}U_z(\beta_j)\mathbf{v}_g$$

$$-C_B^{c*}(\mathbf{k})C_A^v(\mathbf{k}')\sum_j^N e^{i(\mathbf{k}-\mathbf{k}')\cdot R_j^A}U_z(\alpha_j)\mathbf{v}_g^* \Bigg]. \quad (11)$$

Here the $\mathbf{R}_j^B$ and $\mathbf{R}_j^A$ are, respectively, the coordinates of the $B$ and $A$ carbon atoms in the 2D SWNT unit cell. It is noted here that the second term of Eq. (11) is not the complex conjugate of the first term. The vectors $\mathbf{k}'$ and $\mathbf{k}$ are the initial and final wave vectors of the electron, respectively. The $\mathbf{v}_g$ is the dipole vector of a SWNT, and $\mathbf{v}_g$ for each atom is obtained by rotating the dipole vector of the graphite sheet in the $xz$ plane around the $y$ axis in accordance with the chiral symmetry of the nanotube, and $\mathbf{v}_g$ is given by

$$\mathbf{v}_g=U_y(-\pi/6+\theta)\sum_i^3 e^{i\mathbf{k}'\cdot\mathbf{b}_i}\mathbf{b}_i, \quad (12)$$

where $\theta$ is the chiral angle of the nanotube. Here $\mathbf{v}_g$ describes a $B$ atom on the $y$ axis of the tube. To go to another $B$ atom, we rotate $\mathbf{v}_g$ around the $z$ axis by multiplying $\mathbf{v}_g$ by the rotation matrix $U_z$. The dipole vectors show how each atom contributes to the optical absorption for a given polarization vector. In Fig. 3, we show (a) top and (b) side views of the atomic dipole matrix vector (dipole vector) for a (10,10) carbon nanotube at the van Hove singular $k_{ii}$ point for $E_{\text{laser}}=1.8$ eV, that is, $(k_x,k_y)=(3.265,-2.150)$ in units of $a=1$. The dipole vector for each atom has a large $z$ component which contributes to the optical absorption for the parallel polarization $\mathbf{P}=(0,0,1)$, while the small $x$ and $y$ components contribute in the perpendicular polarization, $\mathbf{P}=(1,0,0)$ or $(0,1,0)$. This means that the optical absorption spectra is strong for the parallel polarization.
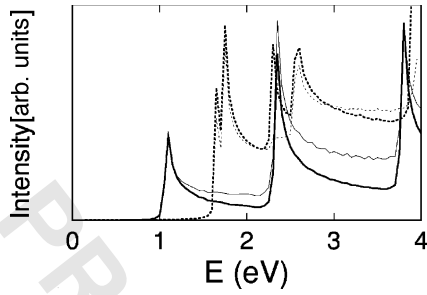
FIG. 4. Energy dependence of the optical absorption of a (10,0) tube with parallel (solid line) and perpendicular (dotted line) polarization. The thick (thin) line is calculated with (without) the matrix element included, and the results show that the van Hove peaks are enhanced by explicit consideration of the matrix element in calculating the optical absorption.

The contribution of each atom to $\mathbf{v}_g$ is multiplied by a phase factor $e^{i(\mathbf{k}-\mathbf{k}')\cdot R_j^B}$ which cancels most of the dipole vectors except for the dipole-allowed transitions. In the case of a vertical transition ($\mathbf{k}=\mathbf{k}'$), only the $z$ components of the dipole vector can be added, and the $x$ and $y$ components are canceled. Thus, when the polarization vector $\mathbf{P}$ is parallel to the nanotube axis, only those transitions (so-called "vertical transitions") are possible which do not change either the electronic $k$ state along the nanotube axis $z$ or the electron wave function symmetry in the circumferential direction (i.e., within the same cutting line). On the other hand, when $\mathbf{P}$ is perpendicular to the nanotube axis, $|\mathbf{k}-\mathbf{k}'|=2/d_t$ $=|\mathbf{K}_1|$, where $\mathbf{K}_1$ is a reciprocal lattice vector of a SWNT,[14,24] a phase change of $\pi$ is introduced into the expression for the optical matrix vectors for the opposite carbon sites, which in turn gives nonzero values for the $x$ and $y$ dipole vectors. Thus the transition from $-E_i^v(k)$ to $E_{i\pm1}^c(k)$ is possible for the cross polarization, which is consistent with previous results.[5]

In Fig. 4 we plot for a (10,0) semiconducting nanotube the optical absorption spectra (thick solid line) and joint density of states (JDOS, thin solid line) for parallel polarization. The thick and thin dotted lines show, respectively, the optical absorption spectra and the JDOS for perpendicular polarization. As is discussed above and given by many previous results,[5,6] the resonant energy positions are different for different polarization directions. When we compare the optical absorption spectra and JDOS, the spectra become more sharp when we explicitly consider the matrix element, though the spectral shape near the singular points for the two cases are similar. It should be mentioned that we do not consider the depolarization effect discussed by Ajiki and Ando[25] in which the optical absorption disappears almost perfectly for the perpendicular polarization. The self-consistent screening effect might not occur in the case of SWNT bundles, since we do observe the perpendicular polarization spectra experimentally in SWNT bundles.[10,11,9,26]

In Fig. 5 we plot the optical absorption matrix element at $k$ points along the $K$-$M$ and $K$-$\Gamma$ lines as a function of the distance of the $k$ vectors from the $K$ point in the 2D BZ. The value of the matrix element in Fig. 5 is given by Eq. (11) for parallel polarization ($z$ component of the optical matrix vec-
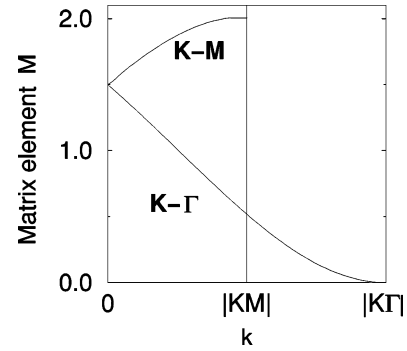


FIG. 5. The optical absorption matrix element for parallel polarization along the high-symmetry lines from $K$ to $M$ and from $K$ to $\Gamma$ as a function of distance of the $\mathbf{k}$ vector from $K$.

tor). It is interesting to see that the matrix element is increasing in the direction from $K$ to $M$ but decreasing from $K$ to $\Gamma$. At the $\Gamma$ point, we do not have an optical absorption of the $\pi$ band. Thus, depending on the $k_{ii}$ position in the 2D BZ of graphite, we can expect a corresponding chirality dependence of the optical absorption intensity.

In Fig. 6, we plot the optical matrix element of Eq. (11) at the van Hove singular point $k_{ii}$ as a function of chiral angle for parallel polarization. The figure is plotted for a given laser energy of 2.41 eV (as is commonly used in Raman experiments) and the $(n,m)$ values are selected within the resonant window of $|E_{ii}-E_{laser}|<0.05$ eV. The solid lines in Fig. 6 correspond to a smooth evaluation of the matrix element along the equienergy contour of 2.41 eV. Each point in Fig. 6 corresponds to a different $(n,m)$ nanotube, and the solid and open dots correspond to metallic and semiconduct-
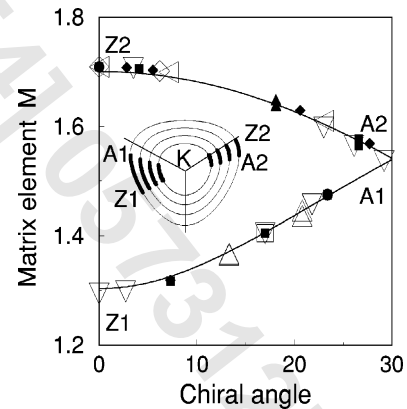


FIG. 6. Chirality dependence of the optical matrix element at the van Hove singular point $k_{ii}$ for 2.41 eV in units of $M=1$ in Eq. (7). The symbols correspond to SWNT's which have a van Hove singularity in a window of 0.05 eV around the laser energy. Solid symbols correspond to metallic tubes and open symbols to semiconducting tubes. The transitions are indicated as follows: $\bigcirc$ $E_{11}$, $\square$ $E_{22}$, $\diamond$ $E_{33}$, $\triangle$ $E_{44}$, $\triangleleft$ $E_{55}$, and $\triangledown$ $E_{66}$. The inset shows the equienergy contours from 1.0 eV to 2.5 eV in steps of 0.5 eV. The possible van Hove singular $k_{ii}$ points are given by the bold part of the equienergy contours. $A1$ and $A2$ show $k_{ii}$ positions and the corresponding matrix element of armchair nanotubes, while $Z1$ and $Z2$ show those of zigzag nanotubes.

ing nanotubes, respectively. From Fig. 6, most points on the two lines in the figure show a chirality dependence of the absorption matrix elements. The relative asymmetric appearance of the two curves in Fig. 6 comes from the fact that the $k_{ii}$ positions exist on inequivalent cutting lines of the 1D BZ relative to the 2D BZ as is shown in the inset, and this inequivalence arises from the trigonal warping effect.[24] In the inset of Fig. 6, we show the $k_{ii}$ positions as the bold parts of the equienergy contours for the laser energies from 1.0 eV to 2.5 eV in steps of 0.5 eV. When the chiral angle $\theta$ of a SWNT changes from $\theta=0$ (zigzag) to $\theta=\pi/6$ (armchair), the $k_{ii}$ position will change in the 2D BZ from $Z1$ (or $Z2$) to $A1$ (or $A2$) of the bold parts of the contours. The corresponding value of the matrix element is shown in Fig. 6. Around the $K$ (or $K'$) point, the value of the absorption matrix element has a threefold rotational symmetry, and depending on the position of the cutting line relative to the $K$ point, the two cases of the bold parts (the long or short ones) can be considered. The chirality dependence of the matrix element comes from the trigonal warping effect of the optical matrix element, as is shown in Fig. 5. In the case of semiconducting nanotubes, the $k_{ii}$ point is along either the $A1$-$Z1$ or the $A2$-$Z2$ curve, depending on their $(n,m)$ values, while in the case of metallic nanotubes, two $k_{ii}$ points appear on the $A1$-$Z1$ and the $A2$-$Z2$ curves. It is noted that the corresponding two $E_{ii}$ values at two $k_{ii}$ position are different from each other, except for armchair nanotubes, for which there is only one $E_{ii}$ value because of the trigonal warping effect.[24] The detailed discussion of the chirality dependence of the optical absorption will be given in the next section. From Fig. 6, it also can be seen that the splitting between the two lines is a maximum for zigzag tubes, which have a chiral angle of zero. In the case of armchair tubes, which have a chiral angle of 30°, the splitting becomes zero. For a given nanotube chirality, except for the armchair case, the width of the splitting increases with increasing laser energy.

## V. DISCUSSION

Although all the present results are based on the standard theory of optical absorption, the results presented here are of particular interest in connection with the recent progress in single nanotube Raman spectroscopy. Here, we discuss possible experimental setups for observing the node phenomena in graphite and the chirality dependence of the optical matrix elements in SWNT's.

The nodes in the absorption matrix element cannot easily be observed by optical absorption spectra, since the optical absorption does not in general select the $k$ vector of the electron. However, we can propose some possible circumstances under which the effect of the nodes in graphite and in SWNT's can be observed. One possibility is to carry out the optical absorption experiment on a nanographite ribbon. The nanographite ribbon is defined as a strip of a graphene layer with a fixed width.[27] Because of the finite size in the direction of the width of the ribbon, the wave vector in the direction perpendicular to the ribbon direction becomes discrete. The situation is similar to that for a SWNT, but the point is

that the dipole vectors $\langle\phi(\mathbf{r}-\mathbf{R}_j)|\nabla|\phi(\mathbf{r}-\mathbf{R}'_j)\rangle$ are parallel to one another on a plane of the ribbon, while that is not the case for the cylindrical surface of SWNT's. Thus we should be able to detect the node by a rotation of the polarization vector in the graphene plane relative to the direction of the nanographite ribbon. The second possibility for observing the node is a study of the polarization dependence of the $D$-band spectra of 2D graphite. In the double resonance Raman theory, the observation of the $D$-band spectra depends on the condition $q\sim2k$ where $q$ and $k$ are the phonon and electron wave vectors, respectively.[17] In this case, all $q$ vectors which satisfy $q\sim2k$ around the $K$ point contribute to yield a broad $D$-band feature. If there is a node in the absorption spectra, some $q$ vectors will not contribute to the $D$-band spectra, and this effect results in a small shift of the $D$-band frequency as a function of the polarization because of the trigonal warping effect of the phonon energy dispersion around the $K$ point. The third possibility is that we can observe the chirality dependence of the resonance Raman intensity, as discussed above.

The chirality dependence of the optical absorption should be observed both in semiconducting and metallic SWNT's, if we can observe their single-nanotube spectra. In the case of semiconducting nanotubes, the $k_{ii}$ positions depend on the $i$ value of $E_{ii}$ and on $(n,m)$ which satisfies $(n-m)=3p\pm1$ ($p$ integer).[24] When $(n-m)=3p+1$, the van Hove singular (vHS) point for $i=1$ exists around the $K$-$\Gamma$ symmetry line, while for $(n-m)=3p-1$, the van Hove singular point for $i=1$ exists around the $K$-$M$ line. The situation becomes opposite for $i=2$. Thus, by comparing the relative intensities corresponding to $E^S_{11}$ and to $E^S_{22}$, we might be able to establish whether the sign is plus or minus for $(n-m)=3p\pm1$. In metallic nanotubes, the $E^M_{ii}$ vHS peaks are split into two peaks, and the higher- and lower-energy peaks are related to the $k_{ii}$ positions around the $K$-$M$ and $K$-$\Gamma$ lines, respectively. Thus the higher-energy peaks have relatively larger optical intensity than the lower-energy peaks whose difference in intensity is the largest for zigzag nanotubes and zero for armchair nanotubes. Actually in the case of armchair SWNT's, for which there is no splitting, we should not observe such an effect. These observations in SWNT's will be possible by using many different laser lines or a tunable laser, which will be useful for assigning $(n,m)$ values using single-nanotube Raman spectroscopy.

## VI. CONCLUSION

In conclusion, we have calculated the optical absorption matrix elements of graphite and SWNT's as a function of **k**. In 2D graphite, the absorption matrix elements for a given polarization and laser energy show nodes on the equienergy lines. Thus we expect a significant polarization dependence of the optical absorption in planar graphite with lower symmetry, such as nanographite or in the case of double-resonance Raman processes in which special **k** points are selected. In the case of nanotubes, the existence of a node is

smeared out by adding contributions from each carbon atom on a cylindrical surface. In accordance with the dipole selection rule, the $z$ or the $x,y$ components of the absorption matrix vector contribute to the absorption, respectively, for the polarizations parallel and perpendicular to the nanotube axis. The absorption matrix element at a van Hove singular point has a chirality dependence which might be observed in intensity spectroscopic measurements (Raman, IR, photoluminescence spectroscopy[28]) made at the single-nanotube level.

[1] H. Kataura, Y. Kumazawa, N. Kojima, Y. Maniwa, I. Umezu, S. Masubuchi, S. Kazama, X. Zhao, Y. Ando, Y. Ohtsuka, S. Suzuki, and Y. Achiba, in *Electronic Properties of Novel Materials—Science and Technology of Molecular Nanostructures*, edited by H. Kuzmany, M. Mehring, and J. Fink, AIP Conf. Proc. No. **486** (AIP, Melville, NY, 1999), pp. 328–332.

[2] S. Kazaoui, N. Minami, R. Jacquemin, H. Kataura, and Y. Achiba, Phys. Rev. B **60**, 13 339 (1999).

[3] M. F. Lin, Phys. Rev. B **62**, 13 153 (2000).

[4] F. J. Garcia-Vidal and J. M. Pitarke, Eur. Phys. J. B **22**, 257 (2001).

[5] H. Ajiki and T. Ando, Physica B **201**, 349 (1994).

[6] I. Bozovic, N. Bozovic, and M. Damnjanovic, Phys. Rev. B **62**, 6971 (2000).

[7] G. S. Duesberg, I. Loa, M. Burghard, K. Syassen, and S. Roth, Phys. Rev. Lett. **85**, 5436 (2000).

[8] J. Hwang, H. H. Gommans, A. Ugawa, H. Tashiro, R. Haggenmueller, K. I. Winey, J. E. Fischer, D. B. Tanner, and A. G. Rinzler, Phys. Rev. B **62**, R13 310 (2000).

[9] Z. Yu and L. E. Brus, J. Phys. Chem. B **105**, 1123 (2001).

[10] A. Jorio, G. Dresselhaus, M. S. Dresselhaus, M. Souza, M. S. S. Dantas, M. A. Pimenta, A. M. Rao, R. Saito, C. Liu, and H. M. Cheng, Phys. Rev. Lett. **85**, 2617 (2000).

[11] A. Jorio, A. G. Souza Filho, V. W. Brar, A. K. Swan, M. S. Ünlü, B. B. Goldberg, A. Righi, J. H. Hafner, C. M. Lieber, R. Saito, G. Dresselhaus, and M. S. Dresselhaus, Phys. Rev. B **65**, 121402(R) (2002).

[12] A. M. Rao, E. Richter, S. Bandow, B. Chase, P. C. Eklund, K. W. Williams, S. Fang, K. R. Subbaswamy, M. Menon, A. Thess, R. E. Smalley, G. Dresselhaus, and M. S. Dresselhaus, Science **275**, 187 (1997).

[13] M. S. Dresselhaus and P. C. Eklund, Adv. Phys. **49**, 705 (2000).

[14] R. Saito, G. Dresselhaus, and M. S. Dresselhaus, *Physical Properties of Carbon Nanotubes* (Imperial College Press, London, 1998).

[15] A. Jorio, R. Saito, J. H. Hafner, C. M. Lieber, M. Hunter, T. McClure, G. Dresselhaus, and M. S. Dresselhaus, Phys. Rev. Lett. **86**, 1118 (2001).

[16] C. Thomsen and S. Reich, Phys. Rev. Lett. **85**, 5214 (2000).

[17] R. Saito, A. Jorio, A. G. Souza Filho, G. Dresselhaus, M. S. Dresselhaus, and M. A. Pimenta, Phys. Rev. Lett. **88**, 027401 (2002).

[18] A. G. Souza Filho, A. Jorio, Anna K. Swan, M. S. Ünlü, B. B. Goldberg, R. Saito, J. H. Hafner, C. M. Lieber, M. A. Pimenta, G. Dresselhaus, and M. S. Dresselhaus, Phys. Rev. B **65**, 085417 (2002).

[19] A. G. Souza Filho, A. Jorio, Ge. G. Samsonidze, G. Dresselhaus, M. A. Pimenta, M. S. Dresselhaus, A. K. Swan, M. S. Ünlü, B. B. Goldberg, and R. Saito, Phys. Rev. B (to be published).

[20] T. Ando, T. Nakkanishi, and R. Saito, J. Phys. Soc. Jpn. **67**, 2857 (1998).

[21] P. L. McEuen, M. Bockrath, D. H. Cobden, Y. G. Yoon, and S. G. Louie, Phys. Rev. Lett. **83**, 5098 (1999).

[22] A. G. Souza Filho, A. Jorio, J. H. Hafner, C. M. Lieber, R. Saito, M. A. Pimenta, G. Dresselhaus, and M. S. Dresselhaus, Phys. Rev. B **63**, 241404(R) (2001).

[23] Z. Yu and L. E. Brus, J. Phys. Chem. B **105**, 743 (2001).

[24] R. Saito, G. Dresselhaus, and M. S. Dresselhaus, Phys. Rev. B **61**, 2981 (2000).

[25] H. Ajiki and T. Ando, J. Phys. Soc. Jpn. **62**, 2470 (1993); **62**, 4267(E) (1993).

[26] A. M. Rao, A. Jorio, M. A. Pimenta, M. S. S. Dantas, R. Saito, G. Dresselhaus, and M. S. Dresselhaus, Phys. Rev. Lett. **84**, 1820 (2000); see also **85**, 3545 (2000).

[27] K. Nakada, M. Fujita, G. Dresselhaus, and M. S. Dresselhaus, Phys. Rev. B **54**, 17 954 (1996).

[28] S. M. Bachcilo, M. S. Strano, C. Kittrell, R. H. Hauge, R. E. Smalley, and R. B. Weisman, Science (to be published).